CHAPTER 4.

CONCENTRATED SOLAR BEAM AND CELL INTERACTIONS

4.1. Introduction

The interaction of light with semiconductor materials and solar cells has been thoroughly described by numerous authors, including those referred to in references 1, 2 and 3. A thorough investigation of the interactions of high intensity concentrated solar radiation with semiconductor materials was presented by the authors in references 4 and 5. In this chapter a brief description of the silicon solar cells that were used in this study will be given. Secondly, an overview of the interactions that are pertinent to this study and that typically take place between a beam of narrowly focused concentrated solar radiation and a solar cell will also be given.

4.2. Silicon Solar Cells

Three types of silicon (Si) solar cells were used in this study: Edge-defined Film Fed Growth (EFG) cells, multicrystalline (MC) cells and point contact concentrator cells made from float zone (FZ) Si material. Both the EFG and MC type cells will be referred to as conventional “flat plate” cells since these types of cells have found widespread use in flat plate photovoltaic (PV) modules. The point contact cell structure was initially only used in concentrator modules. From a materials perspective, both EFG and MC cells can be treated in the

same way as single (mono) crystalline Si cells since their crystal grain size is generally larger than the cell thickness. The illuminated area in the LBIC system is also much smaller than the grain sizes.

During the growth process of the crystalline Si bulk material, boron dopant atoms are introduced to produce a lightly doped (~10^{16} cm^{-3}) *p*-type material. Both flat plate cells have an *n* on *p* structure where a homojunction was formed by dopant diffusion of the Si *p*-type bulk material with pentavalent phosphorous impurity atoms to form a very thin heavily doped (~ 10^{19} cm^{-3}) *n*-type top emitter layer. Nearly all of the volume of a typical crystalline solar cell is thus provided by *p*-type Si. Typical cell thickness range from about 0.5 µm for the *n*-type emitter layer and about 300 µm for the *p*-type base. An important feature of homojunction devices is that there is no material interface at the junction so that losses due to interface states can be avoided. The cell structures are completed by passivating the front surface, adding an anti-reflective coating (ARC), contacting the back surfaces with solid aluminium and screen-printing the front contact fingers with silver paste.

The rear point-contact cell structure was pioneered at Stanford University in 1992 and further developed by the Sunpower Corporation as their HECO range of cells. The cell is made from lightly doped, near intrinsic, *n*-type, high lifetime FZ Si. Heavily doped *n*- and *p*-type regions are formed under the small rear point contacts. Due to the fact that the photogenerated carriers must diffuse to the rear of the cell to be collected, the bulk of the cell material must be very thin, extremely pure and the front surface well passivated.

4.3. Quantum Efficiency and Photocurrent

A primary concern for efficient photovoltaic (PV) devices is the probability that an incident photon of energy E will contribute a single electron to the external circuit of the device at zero junction bias. This probability is represented by the overall external quantum efficiency, QE(E), also known as the spectral response, of a solar cell.

In practice the internal QE(E) may be calculated by using the equation:

$$\text{internal QE}(\mathrm{E}) = \frac{1}{1-R} \cdot \frac{I_{\mathrm{sc}}/e}{P_{\mathrm{L}}/\mathrm{E}} \qquad \textbf{Equation 4.3-1}$$

where e is the elementary charge, I_{sc} is the short circuit current, P_{L} is the power of the incident light and R is the reflection coefficient.

In order for a photon of energy E to contribute an electron to the external circuit of a solar cell, three processes are involved:

a) <u>Photons need to be absorbed.</u> The efficiency with which a photon with energy E is absorbed is best described by the absorption coefficient, $\alpha(\mathrm{E},x)$, of the cell material.

b) The absorption of a photon may lead to <u>the generation of mobile electrons and holes</u> through various generation mechanisms. The monochromatic generation rate of electron-hole pairs, $g(\mathrm{E}, x)$, is amongst others also a function of the absorption coefficient, α. For every carrier generation mechanism there is also an equivalent recombination mechanism causing the loss of an electron or hole through the relaxation of an electron to a lower energy state.

c) <u>Electron hole pairs need to be effectively separated</u> to contribute to the overall photogenerated current of the cell. The balance between the charge

generation rate and the recombination rate determines the number of carriers that are available to be separated and collected by the cell contacts as photocurrent.

The QE is representative of the device structure and the material quality of a solar cell and incorporates factors such as reflection losses from the front surface of the solar cell, carrier generation and recombination rate, absorption coefficient and the probability that a carrier will be collected, η_c(E). The basic form of the photocurrent density, J_{ph}, can thus be written as [2]:

$$J_{ph} = q\int_0^\infty \left[\eta_c(\mathrm{E})\cdot\left(1-R(\mathrm{E})\right)\cdot a(\mathrm{E})\right]\cdot b_S(\mathrm{E})\cdot d\mathrm{E}$$

$$J_{ph} = q\int_0^\infty \mathrm{QE}(\mathrm{E})\cdot b_S(\mathrm{E})\cdot d\mathrm{E}$$

Equation 4.3-2

where b_S(E) is the photon flux density of a beam of monochromatic light, consisting of photons with energy E, that is incident normal to the surface of a solar cell.

Illuminating the solar cell with a beam of full spectrum concentrated solar light will affect the components that make up the photocurrent density, J_{ph}, in Equation 4.3-2 and will be discussed in the following paragraphs.

4.4. Current-Voltage Characteristics

A practical solar cell may operate at various junction biases, V. In an effort to simplify the calculation of the bias dependence of the overall cell current density, two assumptions are normally made:

a) Depletion approximation. To simplify the calculation of the voltage dependence of the recombination currents in the depletion region, we assume that an electric field only exists within fixed distances on either side of the junction. This means that the potential step is rectangular and completely established only by the fixed space charge of the doped materials near the junction, also called the space charge region (SCR). There are thus no free charge carriers in this area. Beyond the junction the *n* and *p* regions are completely neutral with only the variations in the density of the photogenerated minority carriers determining the photocurrent.

b) Superposition approximation. It is assumed that the solution to the total cell current, J(V), consists of completely separate illumination dependant, J_{ph}, and bias dependant, J_{dark}, terms that can simply be added. One of the main assumptions is that the recombination rates in the neutral regions are linear with the photogenerated minority carrier density and not bias dependant at all. The total cell current is thus given by:

$$J(\mathrm{V}) = J_{ph} - J_{dark}(\mathrm{V})$$ **Equation 4.4-1**

When a forward bias is applied to the junction in the dark, the reduction in the potential barrier is given by the term qV and increases the diffusion, J_{diff}, of majority carriers across the junction. Due to the difference in the quasi-Fermi levels in the SCR a net recombination current, J_{SCR}, may appear in the junction region. Majority carrier radiative recombination currents, J_{rad}, may also add to the total dark current and can be added. Ignoring any contributions from parasitic resistances, the total dark current, J_{dark}, is then given by:

$$J_{dark}(\mathrm{V}) = J_{diff,0}\left(e^{\frac{q\cdot \mathrm{V}}{k_B\cdot T}} - 1\right) + J_{SCR,0}\left(e^{\frac{q\cdot \mathrm{V}}{2\cdot k_B\cdot T}} - 1\right) + J_{rad,0}\left(e^{\frac{q\cdot \mathrm{V}}{k_B\cdot T}} - 1\right)$$ **Equation 4.4-2**

where $J_{diff,0}$, $J_{SCR,0}$ and $J_{rad,0}$ are the respective saturation currents.

J_{dark} will thus depend on the relative importance of radiative recombination and recombination in the SCR. J_{dark} can be expressed in the form of the Shockley diode equation:

$$J_{dark}(\mathrm{V}) \approx J_0\left(e^{\frac{q\cdot \mathrm{V}}{n\cdot k_B\cdot T}} - 1\right)$$ **Equation 4.4-3**

where *n* is the ideality factor.

4.5. Absorption of Light

Fig. 4-1 describes the basic interactions of a beam of light with a solar cell material. Consider a beam of monochromatic light that is incident normal to the surface of a solar cell and consisting of photons with energy E and a photon flux density b_s(E). R(E) is the reflectivity of the surface and α is the absorption coefficient of the material. At the surface a portion of the monochromatic light will be reflected, $R\cdot b_s$(E), and the remainder transmitted, b(E). As the light travels inside the material it will be attenuated so that the photon flux density at position x will be given by b(E, x).

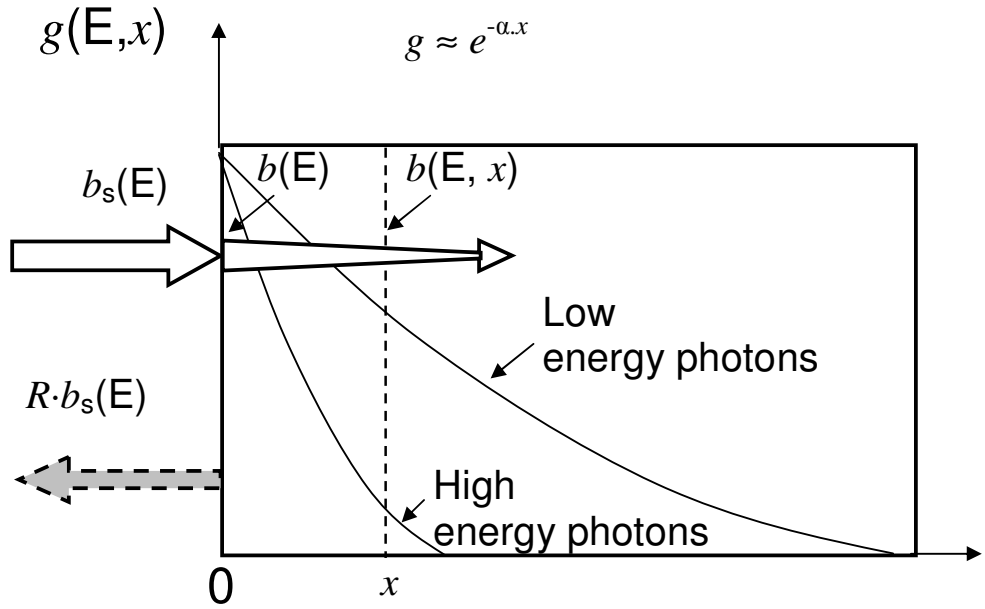

Fig. 4-1. Attenuation, transmission and reflection of incident radiation in semiconductor material. Shown is an approximation for the profile of the carrier generation rate for high and low energy photons.

The attenuation of the incident light beam illustrated in Fig. 4-1 will be characterized by the absorption coefficient, $\alpha(\mathrm{E},x)$, of the cell material for photon energy, E, at position x. The reduction in flux density, db_{E}, after traveling a distance dx inside a material is given by the differential equation:

$$db_{\mathrm{E}} = -\alpha(\mathrm{E},x)\cdot b(\mathrm{E})\cdot dx$$ **Equation 4.5-1**

A solution to this equation gives the flux density of the monochromatic beam after traveling a distance x into the cell material:

$$b(\mathrm{E},x) = b(\mathrm{E})\cdot e^{-\int_0^x \alpha(\mathrm{E},x')\cdot dx'}$$ **Equation 4.5-2**

where $b(\mathrm{E}) = \left(1 - R(\mathrm{E})\right)\cdot b_{\mathrm{s}}(\mathrm{E})$ is the photon flux density just below the surface of the material.

The different processes that absorb electromagnetic radiation in semiconductor materials do so over specific wavelength ranges and will all contribute to the total absorption coefficient. Complete analyses of the energy dependence of $\alpha(E,x)$ for undoped solar cell materials such as Si, Ge, GaAs, AlGaAs and InP are given in references 1, 2 and 3. To aid the discussion on high photon flux density effects, some important results will be reviewed here.

Since the generation of mobile electrons and holes involves inter-band transitions, the absorbed photon energy will have to exceed the bandgap of the material. Of interest is the position and shape of the $\alpha(E)$ curve. The absorption edge for direct bandgap materials (GaAs, AlGaAs, InP) occurs at higher energy values than for indirect bandgap materials (Si, Ge) and corresponds to the energies of their respective bandgaps, E_g. In general, the absorption coefficient for direct bandgap materials depends on the density of occupied valence and unoccupied conduction band states. The additional involvement of phonon assisted inter-band transitions at incident photon energies close to E_g, result in indirect bandgap materials having a softer, slower rising absorption profile than direct bandgap materials at lower photon energies. Direct band transitions without any phonon contributions may become possible at higher photon energies and will usually appear as a change in curvature in α as a function of E [2]. Under high intensity solar spectrum illumination, these direct band transitions may become more frequent due to the increase in the number of higher energy photons. The availability of suitable phonons will also increase due to a process called thermalisation, described in reference 2.

The energy dependence of the absorption process is therefore roughly dependant on the band structure, density of valence and conduction band states and in the case of indirect bandgap materials, on the availability of phonons with suitable energy. At very high photon flux densities the saturation of minority carriers will alter the density of states, which may lead to a change in the energy dependence of various absorption processes. Under high intensity solar spectrum illumination the shape of the $\alpha(E)$ curve may thus be different to that under low intensity illumination.

The absorption coefficient for all the materials generally increases with increasing photon energy and consequently low-energy photons have a longer absorption length ($\frac{1}{e}$) than high-energy photons.

4.6. Quantum Efficiency of a Si Solar Cell

When investigating the LBIC signal that is caused by the interaction between a beam of light with a typical large area *pn* junction solar cell, it is important to consider the contribution to the overall quantum efficiency from the heavily doped front surface, the junction (depletion) region and the lightly doped base regions. In general, the quantum efficiency response at different photon energies, QE(E), reflects the cell design and the semiconductor material quality.

<u>Front surface</u>: Due to their high value for $\alpha(E)$, most of the high energy photons are absorbed and attenuated within a short distance into the cell. The carriers that are subsequently generated close to the front surface of the cell are particularly susceptible to surface recombination. With decreasing incident photon energies the EQ(E) response drops off gradually corresponding to the

drop in $\alpha(E)$ for low energy photons and then drops off sharply close to the bandgap energy, E_g, for Si. The high energy response for QE(E) would thus be more susceptible to the surface recombination velocity than the low energy response.

Base region: Due to their high value for $\alpha(E)$, high energy photons generally cannot penetrate deeply into the lightly doped base regions of a solar cell. With decreasing photon energies, however, the QE(E) response gradually increases. The low energy response for QE(E) would thus be mainly limited by recombination in the back surface and base regions of the cell. With decreasing incident photon energies towards the absorption edge, the EQ(E) response drops off sharply corresponding to the drop in $\alpha(E)$ close to the bandgap energy for Si.

Junction region: Considering the fact that the junction region of the cell lies deeper into the surface than the front region and shallower than the base region, the values for $\alpha(E)$ over the photon energy spectrum will dictate that the contribution to QE(E) would come from intermediate photon energies. The low generation rate in the depletion region would result in the QE(E) response being generally low over these intermediate photon energies. Starting from the high energy side, the QE(E) response would start at a slightly higher photon energy than for the base region. With decreasing photon energies the QE(E) response would rise gradually to relatively low values due to the low generation rate of carriers in the depletion region. Towards the absorption edge, the EQ(E) response again drops off sharply corresponding to the drop in $\alpha(E)$ close to the bandgap energy for Si.

4.7. High Injection Conditions

4.7.1. High Incident Photon Flux Density

The highly concentrated illumination at the beam position on the cell will give rise to high optical injection conditions when the photogenerated carrier density is large compared to the doping density in the base, thus causing localized saturation of minority carriers. In the limit, the electron and hole densities become comparable ($n \approx p$) in the quasi-neutral areas of the *pn* junction and the local carrier lifetimes generally increase. The applicability of Equation 4.4-1 at the illuminated area on the cell is thus limited by two factors: the depletion approximation and the superposition approximation. The non-rectangular form of the space charge profile at high, full solar spectrum illumination levels may limit the first factor. The second factor depends on the linearity of various recombination mechanisms at high flux densities and will be discussed in section 4.8.

4.7.2. External Voltage Bias

At high forward cell bias the volume taken up by the junction increases. If the junction region is weakly doped, as in the case of conventional flat plate cells, more free carriers may occupy the junction region and add to the potential distribution. Since it is likely that $n \approx p$, the trap assisted Shockley-Read-Hall (SRH) recombination rate will be larger [2]. The higher than expected recombination rate in the junction region therefore leads to an underestimation of the recombination current in the SCR, J_{scr}, and thus also to an underestimation of the total dark current suggested by the depletion approximation.

4.7.3. Carrier Transport

Although the carrier distributions under high bias or photon injection conditions will still be shaped by diffusion, the transport mechanism is ambipolar diffusion where the electron and hole motions are coupled together. Carrier lifetimes are generally long in the regime where trap assisted SRH recombination processes dominate at high photon flux densities. This means that the total photo-generated current density may even increase proportionally more than the increase in photon flux density.

4.8. Photogeneration and Recombination at High Flux Densities

The photogeneration rate of electron-hole pairs a distance x from the absorbing surface of a solar cell is shown in Fig. 4-1. When it is assumed that all photons that are absorbed generate free carriers, the spectral photogeneration rate is related to the absorption coefficient through the following relationship:

$$g(\mathrm{E},x) = \alpha(\mathrm{E}) \cdot b(\mathrm{E},x)$$
$$G(x) = \int g(\mathrm{E},x)d\mathrm{E}$$

Equation 4.8-1

where $b(\mathrm{E},x)$ was introduced in Equation 4.5-2.

The total generation rate at x is found by integrating over all incident photon energies that result in free carrier generation. High photon flux densities will usually lead to the saturation of free carriers so that the absorption of more photons may not necessarily generate more free carriers, limiting the applicability of Equation 4.8-1.

When using a narrowly focused beam of monochromatic light that exhibits symmetry in the radial coordinate as an LBIC beam probe, the generation volume is shown in Fig. 4-2 and is assumed to have a Gaussian shape in the lateral dimension. The generation rate for a beam of photons with energy E can then be given at the lateral coordinate r and the depth coordinate, z' in the material as [6]:

$$g(\mathrm{E}, r, z') = \frac{\mathrm{A}(\mathrm{E}, z')}{2\pi\sigma^2} \cdot e^{\frac{r^2}{2\sigma^2(z')}}$$

where $\sigma^2(z') = \sigma_0^2 + \beta^2 z'^2$

Equation 4.8-2

$\mathrm{A}(\mathrm{E}, z')$ is similar to Equation 4.8-1 and gives the depth dependence. σ_0 represents the beam diameter at the surface, and β describes the beam widening and is determined by the refractive index of the semiconductor and the angle of the incident light beam.

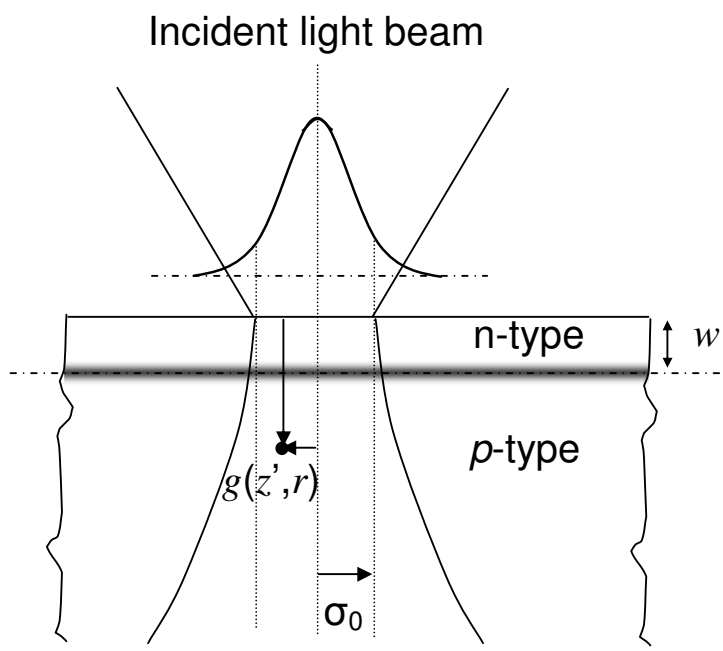

Fig. 4-2. Geometry of the carrier generation profile when using a narrowly focused beam of monochromatic light on a solar cell. The thickness of the very thin diffused surface layer and depletion region are summed up and given by w.

The minority carriers that are generated locally by the light beam diffuse throughout the cell and are collected and swept out by the *pn* junction. In the paper by Marek [6], a full description of a three-dimensional model for the calculation of LBIC signals close to grain boundaries is given.

At high incident photon flux levels the function $A(E, z')$ may deviate from Equation 4.8-1 due to a changing $\alpha(E, x)$ profile. The chromatic aberrations caused by using a refracting lens to focus a full solar spectrum beam onto the solar cell may further cause a significant deviation of the generation volume from having a Gaussian shape. Although Auger (impact ionization) generation and trap assisted generation processes are of relevance to high efficiency solar cells under high flux densities, to exploit these processes specialized cell and band structures are needed, and these are discussed in reference 2.

Referring to section 4.2, the very thin heavily doped emitter layer of the homo-junction structure of the conventional flat plate cells that were used in this study may lead to a very small portion of photogeneration and recombination taking place in the top and depletion regions. In Fig. 4-2, w is very small compared to the total cell thickness, with electron recombination in the lightly doped base *p*-region thus the dominant volume recombination process. Three main recombination mechanisms that are normally identified include radiative, Auger and trap assisted SRH processes. If SRH recombination processes are dominant in a material, even at high illumination levels, superposition should hold; while if radiative and Auger recombination processes become dominant, superposition becomes invalid. Generally, SRH recombination processes are dominant in lightly doped *p*-type material at room temperature. Auger

recombination processes generally dominate in more heavily doped Si or at higher temperatures. Radiative lifetimes in Si are very long and rarely dominate the recombination in a conventional solar cell [2]. Since the electron (minority carrier) diffusion lengths in the lightly doped base layer are normally very long and the recombination is very low, recombination in the surface may become very important.

When Auger and radiative recombination processes are dominant, J_{dark} would not only be a function of junction bias, but also change with incident photon flux density. The implication is that the different recombination processes would cause V_{OC} to vary with light concentration level, X. The variation is given by $\frac{2kT}{q} ln\, X$ for the SRH process, $\frac{kT}{q} ln\, X$ for the radiative process and $\frac{2kT}{3q} ln\, X$ for the Auger process [2].

4.9. Summary

In this chapter a short introduction to the different types of cells that were used in the study was given. Factors that affect the efficient operation of solar cells were identified and their influence at high photon flux densities and changing cell biases discussed. References were made to the use of a beam of narrowly focused monochromatic or concentrated solar light as an LBIC beam probe. The interactions of the beam with the different parts of a solar cell structure were also discussed.

4.10. References

1. S.M. Sze, Physics of semiconductor devices (2nd Edition, Wiley-Interscience, New York 1981)
2. J. Nelson, The physics of solar cells, (Imperial College Press, 2003)
3. S.J. Fonash, Solar cell device physics (Academic Press, 1981)
4. V.M. Andreev, V.A. Grilikhes, V. D. Rumyantsev, Photovoltaic Conversion of Concentrated Sunlight , (John Wiley & Sons Ltd. 1997)
5. F.J. Vorster, On the Evaluation of a Photovoltaic Concentrator System, M.Sc. Dissertation, University of Port Elizabeth, 2001
6. J. Marek, Proceedings of the 17th IEEE Photovoltaic Specialists Conference (1984) 1207 –1212